# Combine Cluster Abundance and Weak Lensing to Derive Cosmological Parameters

Gladys Muthoni Kamau

gladyskamau@u.boisestate.edu

Boise State University

October 22, 2022

**Abstract**

This study synthesizes four main papers with the general aim of deriving two cosmological parameters, matter density ($\Omega_m$) and density fluctuation ($\sigma_8$) using cluster abundance and weak lensing signal. The study uses Dark Energy Survey Year 1 data (DES Y1), the first batch of observatory data released by the DES. Derivation of cosmological parameters highly depends on accurate calibration of cluster mass. The DES Y1 clusters are identified using the redMaPPer algorithm, which is prone to selection effects. For the accurate calculation of the weak lensing mass and constraining the mass–richness relation, the analysis models the systematics which includes projection effects, shear, and photometric uncertainties, cluster member dilution, and cluster miscentering in the estimation of the weak lensing signal. However, the derived cosmological parameters show discrepancies when compared with the results from other probes. The discrepancy primarily originates from the interpretation of the weak lensing signal, implying the existence of systematics yet to be captured in the model. The details of the unmodeled systematics are still a mystery that motivates the need for more observatory and simulated-based research. We also briefly discuss the major upcoming LSST survey and my ongoing research project that aims to shed more light on the identified challenges. In addition, we provide a computing artifact that illustrates the calculation of the weak lensing signal using cosmoDC2. It is publicly available on GitHub.

## 1 Introduction

The field of cosmology has been revolutionized by the discovery of dark matter and dark energy. Edwin Hubble made a critical discovery in 1929 that the Universe is expanding after observing the correlation between a galaxy's redshift and the distance from earth (Bagla, 2009). In 1933, Swiss American astronomer Fritz Zwicky made another discovery of dark matter existence (Zwicky, 2009). He uncovered that the mass of all the stars in the Coma cluster of galaxies made up approximately 1% of the mass required to prevent the galaxies from eluding the cluster's gravitational pull (Zwicky, 2009). It led to a controversy among astronomers until the 1970s when American astronomers Vera Rubin and W. Kent Ford observed a similar phenomenon within a galaxy (Rubin et al., 1980). The mass of the visible stars in a typical galaxy is only about

10% of the mass necessary to keep those stars orbiting the galaxy's center. The observed rotation curve also provided more evidence of dark matter existence (Rubin et al., 1980; de Swart et al., 2017). After astronomers were fully convinced that dark matter exists in the 1980s, theories were put forth and refuted until the dawn of the 21st century when the standard cosmological model was accepted (de Swart et al., 2017; Bertone & Hooper, 2018; Frenk & White, 2012).

Recent experiments indicate a cosmological model that presumes the Universe is made up of three components; dark energy (68%), cold dark matter (27%), and ordinary matter (5%) (Planck Collaboration et al., 2014). Two international teams discovered the dominating Dark Energy in 1998: American astronomers Adam Riess and Saul Perlmutter and Australian astronomer Brian Schmidt (Riess et al., 1998; Schmidt, 2012). Its effect accounts for the accelerating Universe expansion and slowed rate of large structure formation. Dark matter can neither emit, absorb nor scatter light of any wavelength. It can be detected only through its gravitational influence on visible matter. Cosmologists have been trying to comprehend the fundamental physics of dark energy and dark matter particles using galaxy clusters' sensitivity to the expansion of the Universe and the growth of structures.

The hierarchical formation of the structures we observe today dates back to when the Universe was 0.5-1 billion years old when the first stars and galaxies form. Over billions of years, the gravitational accretion of matter has continued resulting in massive gravitationally bound objects such as galaxy groups and galaxy clusters. Galaxy clusters are the largest virialized structures in the Universe. A galaxy cluster constitutes hundreds to thousands of galaxies, intergalactic gas, and mass-dominating dark matter. They reside in the highest peaks of the matter density field, making them powerful probes of cosmology (Graham P et al., 2005).

Galaxy clusters act as gravitational lenses that bend light from distant source galaxies. As a result, the intrinsic shapes of the background galaxies get distorted and their brightness gets magnified. Gravitational lensing has turned out to be a powerful tool for probing galaxy cluster mass, matter distribution and density, and the curvature of the Universe. In estimating the cluster mass using weak gravitational lensing, cosmologists get insights into the trends of physical processes that govern galaxy formation and constrain the cosmological parameters. Dark matter halos have a wide range of mass and formation histories, which are also traced to different galaxy populations, for example, a typical galaxy cluster mass ranges between $10^{13}\mathrm{M}_{\odot}$ to $10^{15}\mathrm{M}_{\odot}$, and the Milky Way is approximately $10^{12}\mathrm{M}_{\odot}$, which belongs to the Local Group. However, weak lensing cosmological analysis is immensely affected by systematic uncertainties.

Over the years, the number and quality of cosmological surveys have drastically advanced to utilize clusters as one of the primary probes in cosmological surveys. This work focuses on cosmological data extracted through an optical imaging survey (DES Year 1) and N-body simulations. The data was later subjected to the redMaPPer algorithm to generate the cluster catalog used for the analysis. The Dark Energy Survey (DES) (Dark Energy Survey Collaboration: Fermilab & Flaugher, 2005), Hyper Suprime-Cam (HSC) survey (Aihara et al., 2018), Canada-France Imaging Survey (CFIS), Kilo Degree Survey2 (KiDS) (De Jong et al., 2015) are some of the completed image surveys with a focus on utilizing galaxy clusters. Future galaxy cluster-based surveys include Rubin Observatory Legacy Survey of Space and Time (LSST) (Abell, Paul et al., 2009), Euclid survey (expected 2023) (Amendola et al., 2018), and the Nancy Grace Roman Telescope (expected 2027) (Pardo & Doré, 2021). In preparation for the LSST observed data analysis, vast N-body cosmological simulations are conducted to generate synthetic galaxy catalogs that assist in developing robust and well-understood analysis pipelines.

The redMaPPer (red-sequence matched-filter Probabilistic Percolation) is an optical cluster finder algorithm designed to detect the over-dense concentration of red sequence galaxies using

multi-wavelength imaging data. Red sequence galaxies, which have no star formation, are mostly found in high-density regions making them excellent tracers of clusters. With the matched filter, the algorithm estimates the probability of each galaxy belonging to a cluster. It then assigns each cluster its richness ($\lambda$), which is the weighted sum of the probability of the red-sequence galaxy members above a fixed luminosity threshold and within the defined cluster radius (Rykoff et al., 2014). Due to projection effects, redMaPPer tends to preferentially select clusters with their major axis aligned along the line of sight.

Weak lensing surveys suffer from both statistical and systematic bias. We expect statistical uncertainties to reduce with advanced surveys and an increased volume of data. However, systematic bias will need to be corrected to improve the accuracy of estimating the galaxy cluster mass. In detail, this work discusses sources and some of the predominant systematic effects such as projection effects, cluster member dilution, triaxiality, photometric redshift, shear errors, and modeling bias. We also explore the estimation of the weak lensing mass after systematics calibration and use cluster observables to constrain cosmological matter density parameters.

The focus of this study was directed by four primary papers. Table 1 shows the title and aim of the analysis for each paper. Due to the complex nature of the cosmological analysis, simulations play a key role to help understand what astronomers directly observe in the sky. The synthesis also used both observational and simulated data to support the derivation of the cosmological parameters.

| **Title** | **Aim** | **Category** | **Data** |
|---|---|---|---|
| Dark Energy Survey Year 1 Results: Cosmological Constraints from Cluster Abundances and Weak Lensing | Derive $\Omega_m$ and $\sigma_8$ parameters | data analysis | Dark Energy Survey: images of $\sim$100 million galaxies |
| Dark Energy Survey Year 1 Results: Weak Lensing Mass Calibration of redMaPPer Galaxy Clusters | Model WL systematics and fit WL mass to constrain mass–richness relation | data analysis | Dark Energy Survey: images of $\sim$100 million galaxies |
| The Impact of Projection Effects on Cluster Observables: Stacked Lensing and Projected Clustering | Quantify the impact of projection effects on cluster clustering, cluster abundance, and cluster lensing. | simulation and modeling | Simulations for the density field of the Universe |
| Optical Selection Bias and Projection Effects in Stacked Galaxy Cluster Weak Lensing | Probe selection bias of stacked weak lensing signal measured from clusters identified using redMaPPer algorithm. | simulation and modeling | Simulations mimicking the Dark Energy Survey |

Table 1: The primary papers.

The study is structured as follows: In section 2 we discuss the current state of galaxy cluster surveys and the main DES Y1 data products used in the analysis. Section 3 introduces the simulation and modeling necessary to support the study. Section 4 describes the systematic effects associated with DES Y1 data products and redMaPPer clusters. In section 5, we present the results of the recent cosmological study, identify the gaps in the study, and a brief summary of my ongoing research project. We conclude in section 6 by summarizing the study.

# 2 Current status of galaxy cluster surveys

The advancement in technology has turned out to be valuable in cosmological surveys, from the size of the telescopes to the depth, resolution, and area of data collection. The Dark Energy Survey (DES) is one of the cluster-based surveys that covered $5000\ deg^2$ of the southern sky and has collected data from the year 2013 to 2019. It used the powerful Dark Energy Camera placed on the Blanco 4m telescope located at the Cerro Tololo Inter-American Observatory in Chile (Flaugher et al., 2015). The telescope has collected over 300 million galaxies. The main aim of DES is to investigate the nature of dark energy and the cause behind the acceleration of the Universe. Most cluster-based cosmological studies revolve around calibrating cosmological parameters to understand the nature of dark energy. In the Abbott et al. (2020) analysis, their core objective is to derive $\Omega_m$ and $\sigma_8$ cosmological parameters from DES Y1, which is discussed further in section 3. DES Y1 is the first batch of observational data released by the DES team after the survey run from August 2013 to February 2014 (Drlica-Wagner et al., 2018). Figure 1 shows a DES deep field image of galaxies that DECam captured during the survey.

Figure 1: Deep sky observation of galaxies. The image is a result of long-time exposure of the DECam on a portion of the sky to show a peek of distant and fainter galaxies. Credit DES/DOE/FNAL/DECam/CTIO/NOIRLab/NSF/AURA

The survey has collected numerous properties of the galaxies but for Abbott et al. (2020) and McClintock et al. (2019) analysis, only four data products are considered from the DES Y1 data as described below:

**Photometry catalog and photometric redshift**. Most astronomical objects are located very far away from us. As a result, astronomers find it challenging to measure the actual distance of the observed objects from Earth. However, the redshift-distance relation, defines that the further a galaxy is from the observer, the more it is redshifted. A redshift of a galaxy is the stretched wavelength due to the expansion of the universe. Astronomers use redshift estimates to estimate

the distance of the galaxy from the Earth. They devised the use of a photometric system, a set of optical filters, to capture the photometry of each galaxy. As the name suggests, photometry is concerned with the measure of how bright a galaxy looks in the sky. The light spectrum of a galaxy experiences a 4000A break, a sharp drop due to the absorption of high-energy radiation from metals in stellar atmospheres. DECam was fitted with g, r, i, z, and Y optical filters that measured the flux of light emitted by galaxies. DES locates the drop of each galaxy on the five passbands to estimate its redshift. The drop of far-located galaxies is observed at longer wavelengths from Earth, more redshifted. This estimation incorporates significant bias, which affects the weak lensing measurements (Hoyle et al., 2018). We will discuss the specific systematics associated with photometric redshift in section 4.

**Shear catalogs**. The shear of a galaxy refers to the distortion of the galaxy image due to weak gravitational lensing. It is one of the direct observables that DES captures. Zuntz et al. (2018) details all the steps involved in generating the shear catalog from converting image data to the galaxy shapes into two quantities; $e1$ and $e2$. The two quantities offer a direct way to measure the weak lensing profile of the clusters. The process of recovering ellipticities from the pixelized data suffers from significant bias, affecting weak lensing analysis accuracy, which we will discuss in section 4.

**Cluster catalogs**. Cluster catalogs form the main basis of all cluster cosmology studies. From the DES Y1 galaxy catalog, the clusters were identified using the redMaPPer algorithm. The algorithm also assigns each cluster redshift and richness estimates (Rykoff et al., 2014). Due to the dominating invisible dark matter, astronomers find it difficult to measure the mass of galaxy clusters directly during surveys. It is therefore imperative to understand how the directly observed cluster property, richness, relates to the estimated cluster mass (McClintock et al., 2019). To increase the signal-to-noise ratio, the galaxy cluster catalog is binned into three redshift and four richness bins spanning the range of $z \in [0.2, 0.65]$ and $\lambda \in [20, \infty]$ respectively. The redshift binning range is limited by photometric data availability while embracing a wider range of bins improves the signal-to-noise ratio of the weak lensing profile. This is clearly shown in Figure 2, where cluster number counts are on the left and weak-lensing masses are on the right. The measurements and associated uncertainties are shown as colored boxes, while the dots correspond to the best-fit model from the estimated parameters. The residual between the data and the best-fit model for each of the bins is shown on the bottom panel.

In the next two years, we expect to have the first batch of the Legacy Survey of Space and Time (LSST) observatory data. LSST is a cluster-based survey that will take place at Vera C. Rubin Observatory and is expected to conduct a synoptic astronomical survey of the southern sky for 10 years. Vera C. Rubin Observatory is currently under construction and will start its operation in July 2023. It will use one of the largest digital cameras, which will be mounted on the 8.4-meter Simonyi Survey Telescope (SST) to provide the widest, fastest and deepest views of the night sky ever observed in astronomical surveys. The Vera C. Rubin Observatory facility is located on the Cerro Pachón ridge in north-central Chile. The survey will focus on addressing four primary areas; the nature of dark matter and dark energy, exploring the changing sky, the formation and nature of our Milky Way galaxy, and creating a directory of the solar system. The LSST Dark Energy Science Collaboration (DESC) is a team of international scientists currently working on scientific pipelines in preparation to derive cosmological parameters using the LSST data. In section 5, I will briefly discuss my current research work, which is part of LSST DESC goals.

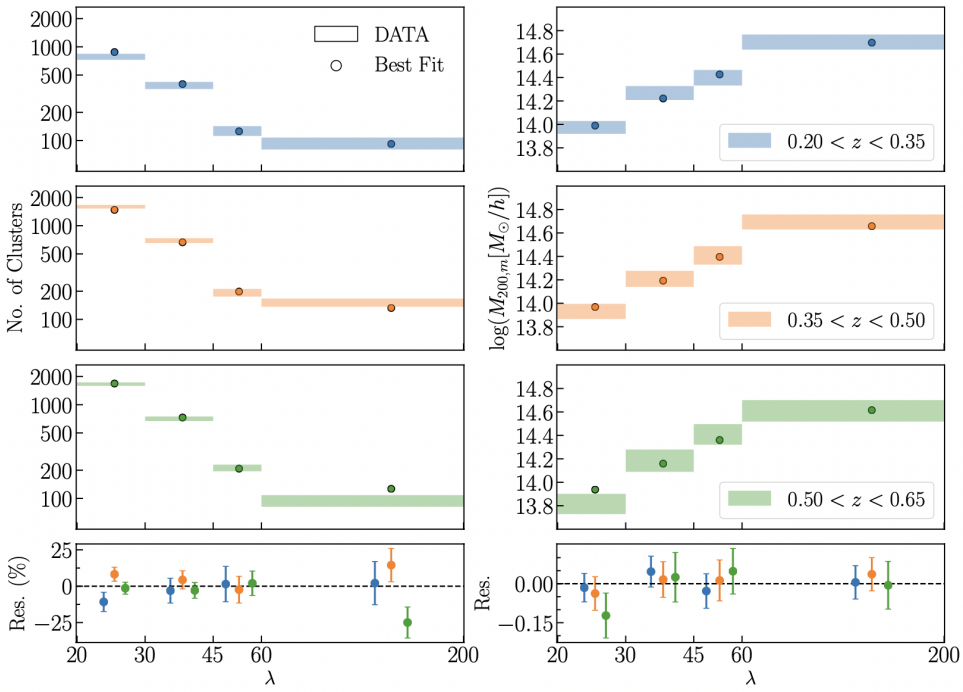


Figure 2: Observed (shaded areas) and best-fit model (dots) for the cluster abundance(left) and mean cluster masses (right) as a function of richness for each of the bins (Abbott et al., 2020). The residual between the data and the best fit is shown on the bottom panel.

# 3 Modeling

In this section, we will discuss how number counts and weak lensing mass is used to infer the two cosmological parameters; $\Omega_m$ and $\sigma_8$. Today's matter density ($\Omega_m$) of the Universe, refers to the average energy density of all types of matter; baryonic and dark matter. The higher the matter density the higher the rate of structure growth. Density fluctuations ($\sigma_8$) refer to the unequal distribution of matter in the early Universe; over-densities and under-densities. A high-density fluctuation implies rapid structure formation during the early times.

## 3.1 Halo Mass Function

Halo mass function shows the number density of dark matter halos per mass range for a given cosmology. It provides the connection between cosmological parameters, cluster abundance and cluster mass. It is the main model used in the analysis to derive the cosmological parameters. Figure 3 clearly shows the evolution of the halo number due to its sensitivity to cosmology. Cluster abundance refers to the number of clusters in the $i^{th}$ richness and redshift bin, (Abbott et al., 2020). Cluster abundance is a widely used cluster property to probe cosmology due to its sensitivity to matter density and density fluctuations (Weinberg et al., 2013). It highly depends on the nature of dark matter and the acceleration of the Universe. From the DES Y1 data, McClintock et al. (2019) estimates cluster mass using gravitational lensing and constrains the mass–richness relation, which is used together with the halo mass function to derive cosmology. The sensitivity of the halo number to cosmology emphasizes the need to accurately calibrate the lensing signal and the mass–richness relation.

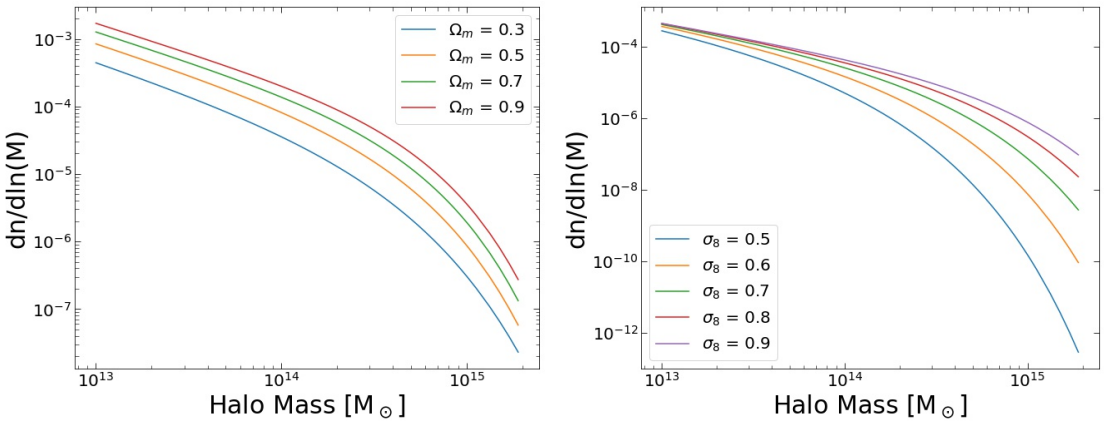


Figure 3: Halo number sensitivity to variation in cosmological parameters. The left-hand panel shows how halo number changes with an increase in matter density value. Higher $\Omega_m$ leads to an increase in the number density of halo masses at low and high mass. The right-hand panel shows how halo number varies with an increase in density fluctuation parameter. Higher $\sigma_8$ leads to a significant increase in the number density of massive halos than less massive halos.

### 3.2 Mass–Richness relation

Inference of the cosmological parameters requires both cluster abundance and halo mass. We can infer the halo mass function with an assumed cosmological model in a simulation-based analysis. However, the DES can only observe number counts as a function of richness and redshift. It is crucial to tightly calibrate the mass–richness relation as it allows us to infer the cluster mass from the observed cluster richness. While reducing the error budget from 11.2% to 5%, McClintock et al. (2019) was able to fit a more accurate weak lensing mass using the stacked weak lensing mass. Using the weak lensing mass, they formulated a model to connect the average cluster mass to the richness as a function of richness and redshift. Section 4 discusses some of the systematic effects that were corrected when fitting the weak lensing mass. These systematics bias the weak lensing and cluster abundance measurements of redMaPPer clusters. In the McClintock et al. (2019) analysis, all the modeled systematic corrections were included in the fitted stacked weak lensing profile of each richness–redshift bin. Section 5 further discusses the results of the Abbott et al. (2020) study where they used the McClintock et al. (2019) results (weak lensing mass estimates) and number counts to derive the cosmological parameters. The mass–richness relation adopted by McClintock et al. (2019) is as follows:

$$\mathcal{M}(\lambda, z) \equiv \langle M|\lambda, z\rangle = M_0 \left(\frac{\lambda}{\lambda_0}\right)^{F_\lambda} \left(\frac{1+z}{1+z_0}\right)^{G_z} \tag{1}$$

where $M_0$, $F_\lambda$ and $G_z$ are the model parameters. The selected pivots are close to the median values; $z_0 = 0.35$ and $\lambda_0 = 40$. $\mathcal{M}$ is the average halo mass as a function of richness and redshift.

## 4 Systematic uncertainties in observations

Accurate derivation of the cosmological parameters highly depends on better calibration of the weak lensing measurements. In the McClintock et al. (2019) analysis, they modeled for both statistical and systematic uncertainties in an attempt to tightly constrain the mass–richness relation. Using simulated data, Sunayama et al. (2020) explored and quantified the impact of

projection effects on cluster lensing and cluster clustering. Cluster clustering is the two-point correlation function that measures how clusters are distributed in the Universe. It describes how clusters are clustered in the Universe. In conjunction with Wu et al. (2022) paper, we can confirm that there exists significant weak lensing systematics, which needs to be included in the calibration of weak lensing mass.

## 4.1 Projection effects and triaxiality

Uncorrelated structures along the line of sight can affect photometric cluster mass proxy due to projection effects. It materializes when the optical cluster finder, redMapper, misidentifies galaxies along the line of sight as genuine members of the cluster, leading to an up-scatter in the estimated cluster richness. Sunayama et al. (2020) provides more evidence of its impact on other clusters observables besides weak lensing signal, posing a challenge to the accuracy of these analyses, particularly calibration of mass–richness relation. More evidence of the impact can be seen in Sunayama & More (2019); Chang et al. (2018) with the observed reduced splash-back radius compared to the theoretical expectations. Splash-back radius is the physical defined cluster boundary. It marks the region of steep slope between the inner and outer region.

Sunayama et al. (2020) generated true and observed cluster samples identified using modified version of the redMaPPer from the mock catalog of red-sequence galaxies. They measured cluster abundance, cluster clustering, and cluster lensing signals from the two samples to quantify the impact of projection effects. To verify their analysis they also compared the results with the theoretical predictions made using the Dark Emulator (Nishimichi et al., 2019). Comparing galaxy cluster count measurements from the true and observed samples showed insignificant discrepancies to probe the impact of projection effects. However, there was a discrepancy between the observed and the expected lensing and clustering signal at a large scale with a boost of 1.2 and 1.4, respectively. The observed signal was computed from the clusters identified with redMaPPer while the expected was from the isotropic halo model. The boost on the clustering signal also depended on the projection depth where the study implemented a standard depth of $\pi_{\rm max} = 500h^{-1}{\rm Mpc}$. Figure 4 and 5 clearly show the observed boosts after comparing the measurements from the observed and true sample and the Dark Emulator predictions.

In investigating the source of the projection effects, Sunayama et al. (2020) found out that $30\%$ of the galaxy clusters identified using the redMaPPer consisted of filaments along the line of sight. This selection bias was caused by the redMaPPer algorithm, which has the tendency of selecting clusters embedded within filaments along the line of sight, leading to richness up-scatter. Changing the line of sight also affected the signal measurements. This implied that both the lensing and clustering are highly anisotropic and the discrepancy cannot be fully explained by the changes in the underlying halos mass distribution. The impact of the projection effects on the two cluster signals affects the interpretation of the mass–richness relation and cluster mass distribution, which might lead to overestimation or underestimation of the halo mass.

## 4.2 Other observational systematics

**Shear and photometric redshift systematics**

These systematics are associated with the shear and photometric redshift catalogs. During the sky survey, the telescope captures galaxies images that are affected by the Point Spread Function (PSF) of the instruments. PSF refers to the impulse response of the optical telescope. It describes how much the telescope has distorted the observed light spread. The PSF also includes the effects of the atmosphere (Amara et al., 2010). The galaxy images get converted to galaxy shapes before estimating the shear measurements that constitute the shear catalog. Galaxy shapes also suffer

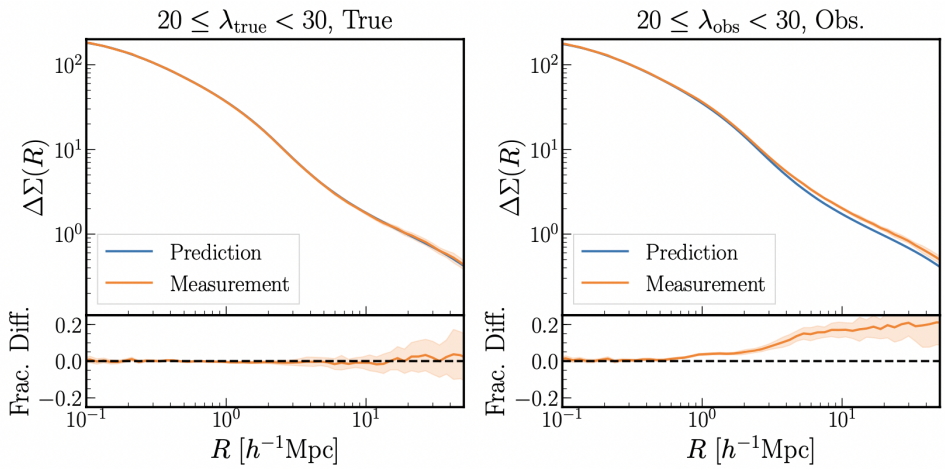


Figure 4: Comparison of the weak lensing signal between the true and observed samples. The weak lensing signal computed from the observed sample shows significant boosts on large scale (Sunayama et al., 2020).

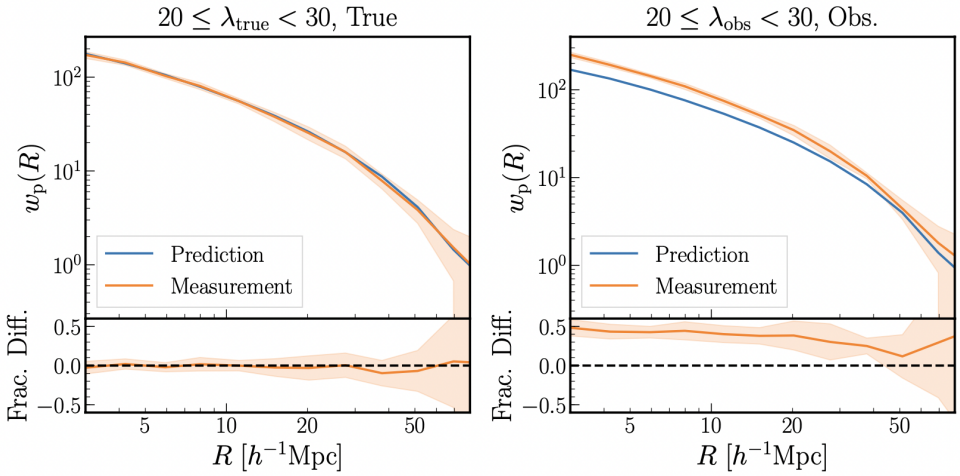


Figure 5: Comparison of the clustering signal between the true and observed samples. The clustering signal computed from the observed sample shows significant boosts on all scales. Note, cluster clustering is always in the two-halo term; large scales as it is measured between distinct halos (Sunayama et al., 2020).

from the dominant noise bias, galaxy blending, which needs to be corrected (Zuntz et al., 2018). Galaxy blending is the overlapping of galaxy images making them occupy the same region of the sky. It is observed as a result of not having enough image resolution. Other sources of shear systematics include the model bias associated with the estimation of the shear measurements. Zhang et al. (2019) also evaluated two independent algorithms for estimating shear measurements which accounted for the systematics associated with the galaxy shapes.

Spectroscopy offers a more accurate approach to measuring galaxy redshifts compared to photometric redshift estimates. However, it is strenuous to measure the spectra of millions of faint galaxies in a weak lensing survey. Due to the depth of DES, it is able to detect a large number of faint galaxies. The telescope time limitation also implies that only a small number of galaxy's redshift can be estimated using spectroscopy. Photometric redshift estimation incorporated bias which needed to be accounted for when calibrating the mass–richness relation. From the DES Y1 data, Hoyle et al. (2018) estimated and validated the photometric redshift catalog using template-based Bayesian Photometric Redshift (BPZ) algorithm (Benítez, 2000). The algorithm

uses Bayesian inference and priors to estimate the photometric redshift. McClintock et al. (2019) included a correction term for both the shear and photometric systematics when computing the lensing profile.

**Cluster member dilution**
Estimation of the lensing signal can be biased due to source galaxies' contamination by foreground galaxies. This is inflicted by the uncertainty associated with photometric redshift estimates. This dilution underestimates the lensing signal, which necessitates the definition of a boost factor to correct the contamination. McClintock et al. (2019) applied a similar approach as Melchior et al. (2017) by using the source galaxy photometric redshift estimates in different radial bins of the cluster to compute the dilution contamination fraction and include a correction term to the estimation of the weak lensing profile. Further elucidation and robustness testing of the approach can be found at (Gruen & Brimioulle, 2017; Varga et al., 2018).

**Cluster miscentering**
Miscentering of clusters refers to when the sky location of cluster centers gets misidentified. It is a major concern that spawns discrepancies between the true and observed underlying matter distribution. In weak lensing surveys, it leads to underestimation of the lensing signal and galaxy number density, biasing the cluster mass estimation. To identify the miscentered fraction, Zhang et al. (2019) and von der Linden et al. (2014) compared the reported centers of clusters identified using redMaPPer to those derived using X-ray of high-resolution data.

# 5 Recent cluster cosmology results from DES and my ongoing work

This section will discuss the recent results of cosmological parameters derived from DES Y1 (Abbott et al., 2020). It will also list the gaps identified during the study. It will cover a summary of the ongoing work where we are using simulated data and the computing artifact.

The Abbott et al. (2020) analysis presents the most recent cluster cosmology results indicating a low value for $\Omega_m$, which leads to a low value of $\sigma_8$. Comparing the two parameter values with other works in the literature—DES $3 \times 2$pt, Plank Cosmic Microwave Background (CMB), Baryon Acoustic Oscillations (BAO) measurements, and supernovae data—conveys a significant tension as shown in figure 6. This tension implies incomplete modeling of the systematics or the underlying fundamental physics. Further investigation by comparing analysis done with X-ray data and mass–richness relation constrained from clusters identified using SZ implies weak lensing interpretation is the source of the observed discrepancy.

Increasing projection effects, assessing the impact of baryonic processes, cluster percolation, and re-evaluating cluster miscentering are some of the tested possible solutions. Although doubling the projection effects reduced the tension, none of the listed possible solutions fully accounts for the discrepancy. Rerunning the analysis using $\lambda > 30$ significantly reduces the discrepancy and yields results consistent with X-ray and SZ-selected cluster catalogs. Eliminating low richness from the analysis suggests a richness-dependent offset not captured in the model.

## 5.1 Gaps

- The source of the discrepancy between DES results and other probes is not clearly known, increasing the need for further study. People have tried several techniques such as investigating the incompleteness of the redMaPPer catalog. However, comparing with X-ray clusters at low redshift suggests that the level of incompleteness is unfeasible to explain

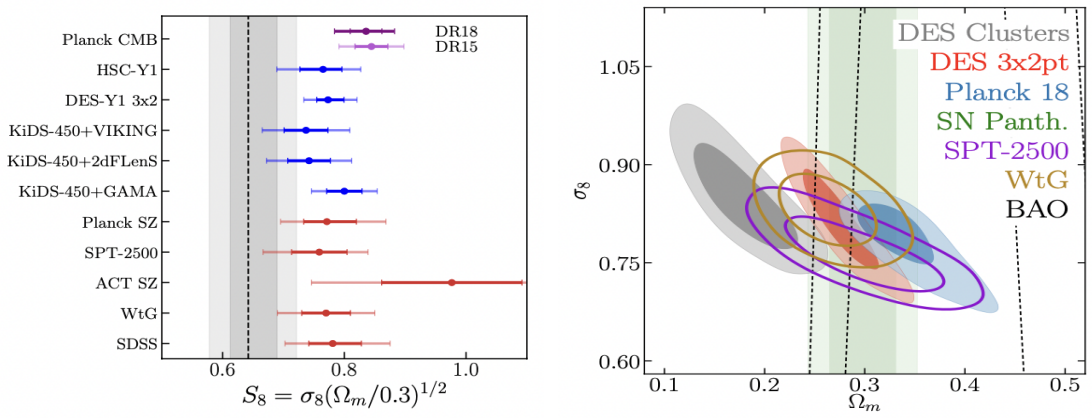


Figure 6: Comparison between DES results with other probes. The left panel compares the structure fluctuation parameter, $S_8$, with existing literature based on cluster abundances (red), weak lensing, galaxy clustering (blue), and CMB (purple) analysis. The grey shaded area shows the derived $S_8$ in the (Abbott et al., 2020). The right panel shows the $\sigma_8 - \Omega_m$ tension when compared with other probes. The gray contour is the derived $\sigma_8 - \Omega_m$ plane using number counts and weak lensing from DES Y1.

the discrepancy. Reducing the cluster percolation increases the number of clusters by $1\%$ but is far from what is required to reconcile the tension. Assessing the impact of projection effects by doubling it slightly reduces the tension between DES results and DES $3 \times 2$pt. However, further increase of projection effects yields no additional relaxation of the tension. A large contamination fraction of spurious clusters is another systematic that can cause the discrepancy. However, repeating the analysis while correcting for the large contamination fraction does not reduce the tension. The baryonic effect is also eliminated as a source of discrepancy. Analysis done with hydrodynamic simulation show that bias caused by baryonic effect is small to reconcile DES results with DES $3 \times 2$pt. Miscentering is another richness-dependent systematic but comparing it with the X-ray data makes it an improbable cause of the discrepancy. Dropping the lowest richness bin reduces this discrepancy, however, the study opens the possibility that such bias might affect other low-mass objects. There are ongoing studies with alternative methods like using stellar mass as a mass proxy which is richness-independent.

- Projection effects is a dominant and not well-understood systematic effect. The results from Sunayama et al. (2020) and Wu et al. (2022) vary on the quantification of selection bias. In Wu et al. (2022), the results indicate a higher selection bias compared to Sunayama et al. (2020) and is observed at small and large scales. Selection bias is negligible at small scales in the Sunayama et al. (2020) paper. Both studies are conducted using different catalogs. This opens the question of whether this difference is causing the varying results. Projection effects is expected to be a major challenge in the LSST observatory data analysis due to the depth of the survey, emphasizing the need for further study of the systematic.

Alternative methods to use different cluster mass proxies such as stellar mass might offer a less biased cluster mass calibration (Palmese et al., 2020); the impact of the projection effect may be small (Bradshaw et al., 2020). Both Abbott et al. (2020) and McClintock et al. (2019) emphasize on the importance and necessity of identifying and quantifying the systematic effects to improve future analysis. Further analysis by combining both observational and simulation-based studies will enlighten astronomers more on the mysteries raised by DES Y1 cluster abundance and lensing data.

One of the LSST DESC's goals is to create, verify and maintain the simulation-based analysis. To support this goal, LSST DESC intends to carry out Data Challenges, which will also guide the development of necessary software pipelines. DC2 is the first multi-purpose LSST data set being utilized to build prototype analysis pipelines. Currently, I am working on CosmoDC2, which is the first product of DC2. CosmoDC2 is a vast simulated galaxy catalog mimicking the expected LSST observatory data. It is based on an N-body simulation covering $440\ deg^2$ of the sky area to a redshift of 3. The catalog comprises several properties of galaxies such as galaxy shear, host halo information, stellar mass, morphology, and broadband filter magnitudes. CosmoDC2 has gone through a multitude of validation tests to support the scientific objectives of the anticipated LSST DESC probes. LSST DESC is currently exploring the primary five cosmological probes that LSST supports. The probes include weak gravitational lensing, galaxy clustering, and clusters of galaxies, which give insight into the dark matter structures and astronomical objects' growth rate. Cosmological distance measurements are provided by Type Ia Supernovae, strong lens systems, baryon acoustic oscillations, and gravitational wave sources, which are independent of structure evolution. For an accurate derivation of cosmology using LSST data, the probes will highly depend on well-corrected systematics while comparing the results to the existing theory and models.

My current research project aims to quantify the optical selection bias and projection effect in cluster gravitational lensing using CosmoDC2 data. The simulated extragalactic catalog comes in two parts; galaxies catalog (CosmoDC2) and cluster catalog identified using redMaPPer (CosmoDC2 redMaPPer). CosmoDC2 also contains properties about the host halo such as halo mass, halo ID, etc. Limiting the halo mass to a minimum of $10^{13}\mathrm{M}_{\odot}$, I computed the weak lensing signal from the underlying halo distribution and the richness-selected clusters. I intend to compare the weak lensing signal computed to quantify the selection bias. The project also aims to compare different mass proxies such as the stellar mass and identify less biased ones. This study will improve cluster cosmology and give more insights into some of the identified challenges while preparing for the upcoming LSST observatory data.

## 5.2 Computing Artifacts

The computing artifact entails three main Jupiter notebooks available at the public GitHub link. It illustrates how to extract, and measure the weak lensing profile of the galaxy clusters and start probing the selection bias systematic effect. The analysis is simulated-based. The cosmoDC2 catalog is extracted using Generic Catalog Reader (GCR). GCR is an open-source python package that creates a user interface to access generic table-like catalogs like cosmoDC2. The richness cluster catalog and halos are extracted using GCR in the National Energy Research Scientific Computing Center (NERSC). NERSC is a primary scientific computing facility in the U.S. Department of Energy. The simulated cluster catalogs are mirrored in NERSC, as a storage facility. It also provides computational resources. Access to NERSC is a requirement to be able to run the notebooks. More details of the computing artifact can be found at the GitHub link provided.

# 6 Conclusion

We have studied the critical importance of galaxy clusters in cosmology in the analysis. The synthesis focuses on using cluster abundance, and weak lensing mass to derive cosmological parameters from the DES Y1. The study also includes investigating and modeling the systematic effects that bias the cluster abundance and weak lensing mass. The clusters from the DES Y1 were identified using the redMaPPer algorithm. For further investigation on the systematics,

projection effects, we study Sunayama et al. (2020) and Wu et al. (2022), which confirm the existence of projection effects that need to be modeled. The study incorporates systematics correction in the estimation of the weak lensing mass and later constrains the mass–richness relation. However, the derived cosmological parameters exhibit discrepancies when compared to other probes. Further probe of the derived low $\Omega_m$ indicates that the observed tension originates from wrong interpretation of the weak lensing mass. This implies there are systematics yet to be captured by the model. This motivates the need for further observational and simulated-based analysis.

# References


Abbott T. M. C., Aguena M., et al., 2020, Phys. Rev. D, 102, 023509

Abell, Paul A., et al., 2009, p. arXiv:0912.0201

Aihara H., et al., 2018, Publications of the Astronomical Society of Japan, 70, S4

Amara A., Réfrégier A., Paulin-Henriksson S., 2010, MNRAS, 404, 926

Amendola L., et al., 2018, Living reviews in relativity, 21, 1

Bagla J. S., 2009, arXiv e-prints, p. arXiv:0904.2633

Benítez N., 2000, ApJ, 536, 571

Bertone G., Hooper D., 2018, Reviews of Modern Physics, 90, 045002

Bradshaw C., Leauthaud A., Hearin A., Huang S., Behroozi P., 2020, MNRAS, 493, 337

Chang C., et al., 2018, The Astrophysical Journal, 864, 83

Dark Energy Survey Collaboration: Fermilab University of Illinois at Urbana-Champaign U. o. C. L. B. N. L. C.-T. I.-A. O., Flaugher B., 2005, International Journal of Modern Physics A, 20, 3121

De Jong J., et al., 2015, Astronomy & Astrophysics, 582, A62

Drlica-Wagner A., Sevilla-Noarbe I., Rykoff E. S., et al., 2018, ApJS, 235, 33

Flaugher B., Diehl H. T., Honscheid K., et al., 2015, AJ, 150, 150

Frenk C. S., White S. D. M., 2012, Annalen der Physik, 524, 507

Graham P S., Kneib J., Smail I., Mazzotta P., Ebeling H., Czoske O., 2005, MNRAS, 359, 417

Gruen D., Brimioulle F., 2017, MNRAS, 468, 769

Hoyle B., et al., 2018, MNRAS, 478, 592

McClintock T., et al., 2019, MNRAS, 482, 1352

Melchior P., et al., 2017, MNRAS, 469, 4899

Nishimichi T., et al., 2019, ApJ, 884, 29

Palmese A., et al., 2020, MNRAS, 493, 4591

Pardo K., Doré O., 2021, Phys. Rev. D, 104, 103531

Planck Collaboration Ade P. A. R., Aghanim N., Armitage-Caplan C., Arnaud M., Ashdown M., et al., 2014, A&A, 571, A12

Riess A. G., et al., 1998, AJ, 116, 1009

Rubin V. C., Ford W. K. J., Thonnard N., 1980, ApJ, 238, 471

Rykoff E. S., et al., 2014, ApJ, 785, 104

Schmidt B. P., 2012, Reviews of Modern Physics, 84, 1151

Sunayama T., More S., 2019, MNRAS, 490, 4945

Sunayama T., et al., 2020, MNRAS, 496, 4468

Varga J., et al., 2018, A&A, 617, A83

Weinberg D. H., Mortonson M. J., Eisenstein D. J., Hirata C., Riess A. G., Rozo E., 2013, Phys. Rep., 530, 87

Wu H.-Y., et al., 2022, MNRAS, 515, 4471

Zhang Y., et al., 2019, MNRAS, 487, 2578

Zuntz J., et al., 2018, MNRAS, 481, 1149

Zwicky F., 2009, General Relativity and Gravitation, 41, 207

de Swart J. G., Bertone G., van Dongen J., 2017, Nature Astronomy, 1, 0059

von der Linden A., et al., 2014, MNRAS, 443, 1973